Environ. Sci. Technol. **2010,** *44,* 6887–6892

Fenton Activity and Cytotoxicity Studies of Iron-Loaded Carbon Particles

BRIAN PEEBLES,[†] AMBER NAGY,[‡] W. JAMES WALDMAN,[‡] AND PRABIR K. DUTTA*,[†]

Department of Chemistry, The Ohio State University, 100 W. 18th Avenue, Columbus, Ohio 43210, and Department of Pathology, The Ohio State University College of Medicine, 4160 Graves Hall, 333 W. 10th Avenue, Columbus, Ohio 43210

Received April 20, 2010. Revised manuscript received July 11, 2010. Accepted July 25, 2010.

The chemical and biological properties of iron-loaded manufactured carbon nanoparticles (Flammruss 101) were contrasted with those of an iron-loaded synthetic carbon particle. X-ray photoelectron spectroscopy was used to characterize the iron on the carbon particles. Production of hydroxyl free radicals via the Fenton reaction was monitored by electron paramagnetic resonance spectroscopy. The iron-loaded synthetic carbon particles produced a positive Fenton response, whereas the iron-loaded manufactured carbon particles did not. The source of the Fenton activity of the synthetic carbon particles is proposed to be a soluble iron compound that was formed during the synthesis of the particle. A likely candidate for the soluble iron species is Fe_2F_5, which was synthesized and its properties were examined. Higher toxicity of Fe_2F_5 toward murine macrophages compared with other simple iron salts was attributed to soluble iron that was stabilized by the fluoride ligand. The cytotoxicity of manufactured carbon particles toward murine macrophages decreased or remained unaltered upon impregnation with iron compounds.

Introduction

Predicting and determining the potential toxicity of nanomaterials is important for the health and safety of employees involved in their manufacture, as well as consumers who are exposed to nanomaterials (*1*). As a redox-active metal, iron can cause oxidative damage, e.g. with hydrogen peroxide it can react to produce hydroxyl radicals through the Fenton and Haber−Weiss reactions (*2, 3*). These radicals can cause membrane disruption, lipid peroxidation, and mutation of DNA, and can lead to diseased states (*4*). Some manufactured nanoparticles, such as carbon nanotubes, can contain 30% metals by weight (*5*).

A challenge in studying the toxicity of manufactured particulates is their chemical complexity. For example, with metal-containing carbon particles, the presence of adsorbed organics can facilitate free radical production (*6*). To isolate the effect of iron chemistry on the toxicity of carbon particles, Kristovich et al. prepared iron-loaded synthetic carbon particles (*7*). In this study, we focus on the Fenton chemistry of iron-loaded manufactured carbon particles (Flammruss 101) and their cytotoxicity. We contrast the changes with metal loading of commercial carbon particles with the synthetic carbon particles.

Experimental Section

Synthesis. *Synthesis of Iron-Loaded Synthetic Carbon Particles.* Micrometer-sized synthetic carbon particles containing iron were synthesized using a published procedure (*7*). Briefly, a cross-linked phenol-paraformaldehyde copolymer was made inside a Fe(II)-zeolite Y, pyrolyzed at 850 °C, and the zeolite was removed by etching in 49% hydrofluoric acid. The etched carbon was washed with water, rinsed with absolute ethanol, and dried at 50 °C under vacuum.

Synthesis of Iron-Loaded Manufactured Carbon Particles. Carbon black (Flammruss 101, Degussa) was wet impregnated with 10% iron by weight as Fe(II) acetate (>95%, Acros Organics), a mix of Fe(II) acetate and Fe(III) nitrate nonahydrate (>98%, Mallinckrodt), or as $Fe_2F_5 \cdot 2H_2O$, and the water was evaporated under vacuum in ambient conditions (overnight), followed by drying under vacuum at 75 °C.

Preparation of Fe_2F_5. $Fe_2F_5 \cdot 2H_2O$ was prepared using a procedure adapted from Hall et al. (*8*). One gram of iron powder (>99%, J. T. Baker) was added to 20 mL of 49% HF with vigorous stirring. A dark red precipitate formed within a few days. This precipitate was washed with absolute ethanol and dried at ambient temperature.

Characterization. Ten μL of carbon particles (concentration 10 mg/mL) in water was added to 990 μL of solution containing 90 mM 5,5-dimethyl-1-pyrroline *N*-oxyl (DMPO, Dojindo Molecular Technologies) and 0.6% hydrogen peroxide. EPR spectroscopy was done using a Bruker ESP300 spectrometer, at a modulating frequency of 100 kHz, with microwave frequency and power set to 9.77 GHz and 20 mW, respectively.

Dynamic light scattering was done using a Coherent Innova 900 argon laser (514 nm) and a Brookhaven Instruments photon correlator. Particle size distributions were calculated using the CONTIN algorithm. A Kratos Ultra Axis X-ray photoelectron spectrometer with an Al Kα monochromatic source was used for XPS. Deconvolution and quantification were performed using CasaXPS software. X-ray powder diffraction was performed using a Bruker D8 Advance diffractometer with a Cu Kα source. Atomic absorption spectroscopy was performed using a Buck Scientific Accusys 211 spectrometer. Thermogravimetric analysis was done with a Perkin-Elmer Pyris thermogravimetric analyzer. The Raman spectrum was collected using a 633 nm laser on a Renishaw InVia Raman microprobe.

Dissolved iron(II) contents were determined by chelation with 1,10-phenanthroline and UV−visible spectroscopy (Shimadzu UV 2501 PC). Solutions of Fe_2F_5, Fe(III) nitrate, and Fe(II) acetate solutions in serum-free cell culture media were made without phenol red or gentamycin (X-Vivo 15, Lonza Inc., Walkersville, MD) at concentrations of 18.5, 42.5, and 14. 0 μg of Fe/mL, respectively. The solutions were sonicated and centrifuged at 20 000 rpm. Twenty μL of 10% 1,10-phenanthroline solution in absolute ethanol was added to 3 mL of the supernatant and absorbance was measured at 510 nm. Atomic absorption spectroscopy was carried out on the supernatant to determine total dissolved iron.

In Vitro Testing of Particles and Iron Compounds. *Cells for In Vitro Testing.* Murine alveolar macrophages of the MH-S cell line were acquired from the American Type Collection. They were cultured at 37 °C in 5% CO_2 in RPMI 1640 cell culture medium (Gibco), 10% fetal bovine serum (Atlanta

* Corresponding author e-mail: dutta.1@osu.edu.
[†] Department of Chemistry, The Ohio State University.
[‡] Department of Pathology, The Ohio State University College of Medicine.

10.1021/es101250s
Published on Web 08/09/2010

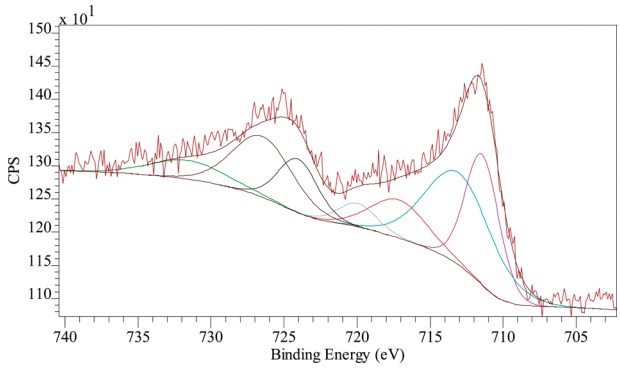

FIGURE 1. X-ray photoelectron spectrum of Flammruss 101 impregnated with 10% iron(II) acetate, in the Fe 2p region, along with the deconvoluted peaks.

Biologicals), and 0.1% penicillin−streptomycin (Gibco). The cell suspension was placed in 24-well plates at a concentration of approximately 5×10^4 cells per well. The cells were acclimated for 24 h prior to particle exposure.

Cell Exposure to Particles. Particle suspensions were made at a concentration of 2 mg/mL using phosphate buffered saline. The suspensions were sonicated and immediately added to the cultured cells (volume 600 μL) at the concentrations indicated in each experiment. Plates were then centrifuged for 2 min at 1400 rcf. After 8, 12, and 24 h supernatant samples were harvested, centrifuged at 16 000 rcf, and transferred to new tubes. Samples were stored at −80 °C until cytotoxicity assays were performed.

Lactate Dehydrogenase Assay for Cytotoxicity. Cell death was assessed by quantifying lactate dehydrogenase (LDH). Cells were treated with PBS only (negative control) or with cell culture medium containing 1% Triton-X 100 (Sigma) which completely lyses cells for a positive control. LDH detection kits (Clontech) were used according to the manufacturer's directions, and plate optical densities (OD) were read at 490 nm with reference wavelength of 600 nm using a BioTek FL600 plate reader (Biotek).

Results

Characterization. *Characterization of Flammruss 101.* The EPR spectrum of solid Flammruss 101 (Figure 1 in Supporting Information) has a peak centered at $g = 2.0112$, consistent with reported spectra (*9*). Dynamic light scattering indicates that Flammruss 101 particles in water had effective diameter of 200−450 nm compared to the primary particle size of ∼100 nm (Figure 2 in Supporting Information). In phosphate buffered saline solution, the size increased to 750−850 nm.

Characterization of Iron-Loaded Flammruss 101. The X-ray photoelectron spectrum in the Fe 2p region of Flammruss 101 impregnated with iron(II) acetate is shown in Figure 1. The deconvoluted spectrum in the Fe $2p_{3/2}$ region indicates that the iron on the surface is approximately 42% Fe(II) (711.4 eV binding energy) and 58% Fe(III) (713.0 eV). Other peaks are assigned as Fe(II) and Fe(III) satellites at 717.2 and 720.0 eV respectively, Fe(II) and Fe(III) $2p_{1/2}$ peaks at 724.0 and 726.5 eV, respectively, and a satellite peak at 731.6 eV (*10*).

Dynamic light scattering shows that particles impregnated with iron were ∼200 nm larger in diameter than untreated Flammruss 101 in phosphate buffered saline.

Figure 2a shows that when Flammruss impregnated with iron(II) acetate was placed in a solution of hydrogen peroxide and DMPO, the signal from the DMPO−OH adduct was near noise level. Adding 1 mM ascorbic acid to the solution resulted in a significant increase in the quartet of peaks from the DMPO−OH adduct, as shown in Figure 2b.

Characterization of Iron-Loaded Synthetic Carbon Particles. The X-ray photoelectron spectrum of iron-loaded synthetic carbon is shown in Figure 3. The fitted spectrum

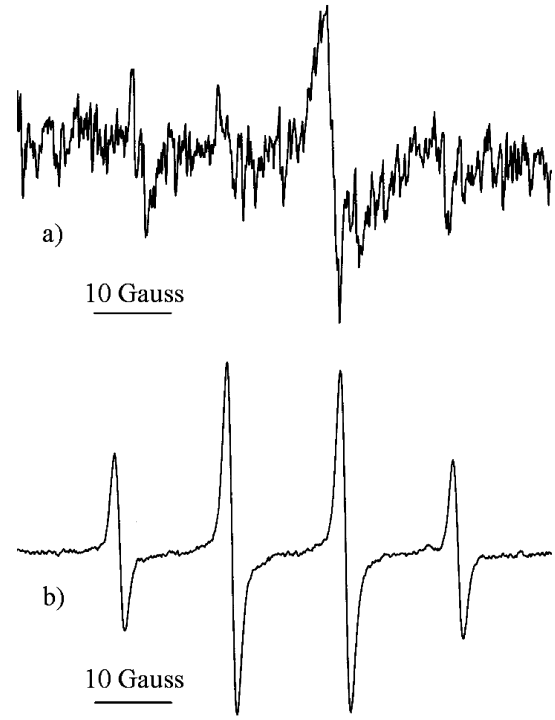

FIGURE 2. EPR spectra of (a) Flammruss 101 impregnated with 10% iron(II) acetate, suspended in hydrogen peroxide and DMPO, and (b) with 100 ppm ascorbic acid added to the solution. All samples are in aqueous hydrogen peroxide and DMPO.

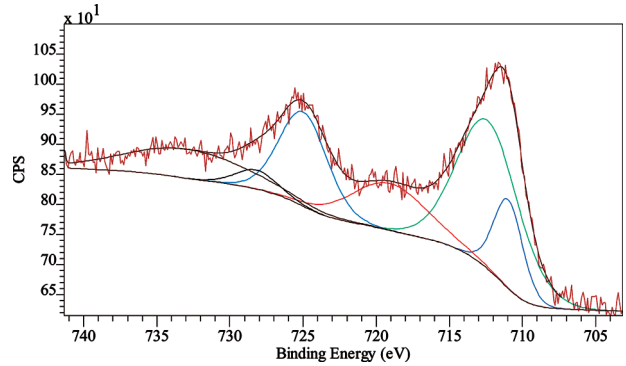

FIGURE 3. X-ray photoelectron spectrum of iron-loaded synthetic carbon, in the Fe 2p region, along with the deconvoluted peaks.

shows that the iron on the surface is approximately 22% Fe(II) (711.0 eV) and 78% Fe(III) (712.4 eV).

The EPR spectrum of the iron-loaded synthetic carbon in hydrogen peroxide and DMPO is shown in Figure 4a. This pattern indicates that hydroxyl free radicals are produced, consistent with the findings of Long et al. (*11*). Figure 4b shows that upon washing the particles in water, the Fenton activity is transferred to the supernatant, with eventually the remnant particles in Figure 4c only showing a trace of Fenton activity.

Characterization of $Fe_2F_5 \cdot 2H_2O$. The X-ray diffraction pattern for the mixed-valence iron fluoride prepared by dissolution of iron powder in hydrofluoric acid matches well with that of $Fe_2F_5 \cdot 2H_2O$ (Figure 3 in Supporting Information). Atomic absorption spectroscopy indicates ∼46% iron by weight, consistent with the composition of $Fe_2F_5 \cdot 2H_2O$. The weight loss of 14.7% occurring between 190 and 270 °C matches that of the dihydrate, $Fe_2F_5 \cdot 2H_2O$ (*12*) (Figure 4 in Supporting Information).

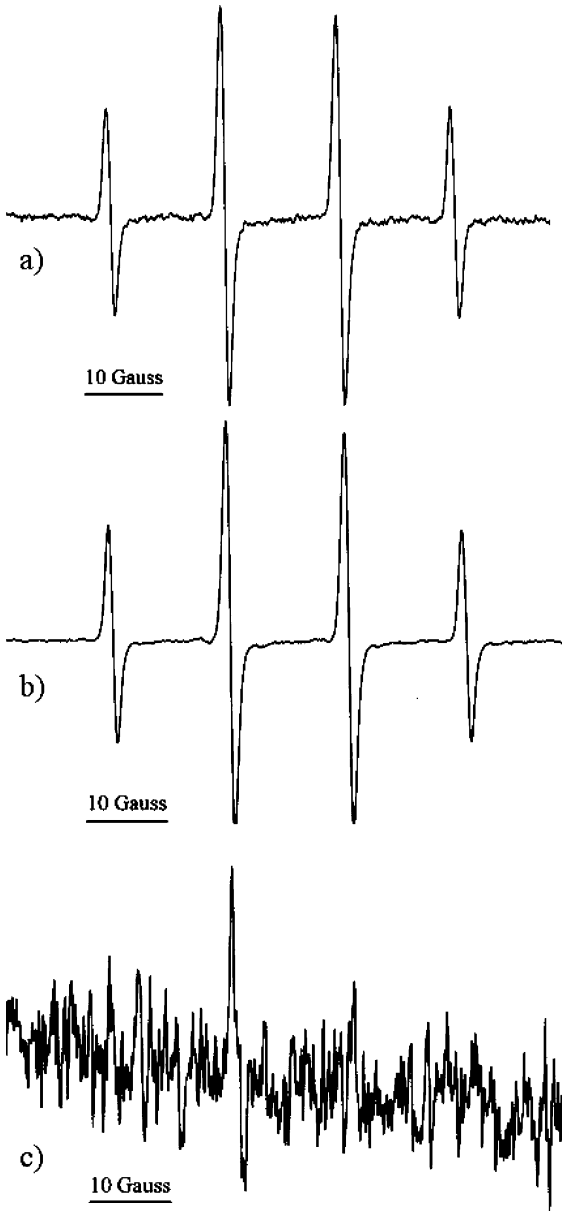

FIGURE 4. EPR spectra of (a) suspended iron-loaded synthetic carbon particles, (b) the supernatant taken from washing the same carbon particles in nanopure water, and (c) suspended iron-loaded synthetic carbon particles after washing with water. All samples are in aqueous hydrogen peroxide and DMPO.

The Raman spectrum of Fe_2F_5 is shown in Figure 5 of Supporting Information. X-ray diffraction, Mossbauer spectroscopy, and magnetic properties of Fe_2F_5 suggest the formula $[Fe^{2+}]$ $[FeF_5(H_2O)]^{2-}$ (*13*). The bands at 493 and 410 cm^{-1} are assigned to the Fe−F stretching vibrations in the $[FeF_5(H_2O)]^{2-}$ molecule (C_{4v} geometry) based on the Raman spectrum of FeF_6^{3-} (*14*). Other bands at 224 and 290 cm^{-1} are assigned to F−Fe−F bending modes, and the bands at 609 and 657 cm^{-1} are assigned to the librational motion of water and Fe−O stretch, respectively. EPR spectrum of Fe_2F_5 in aqueous solution with hydrogen peroxide and DMPO is shown in Figure 5. The formation of the hydroxyl adduct suggests that $Fe_2F_5 \cdot 2H_2O$ is a Fenton active agent, in its native form.

Cytotoxicity Assays. Cytotoxicity results for cells exposed to Flammruss are shown in Figure 6. Focusing on the 12-h exposure, it shows that with 38, 76, and 115 μg of carbon per mL, 60−100% of cells were dead. Impregnation of Flammruss

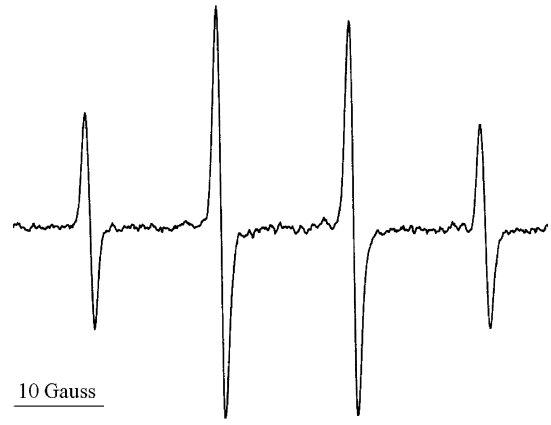

FIGURE 5. EPR spectrum from 1.8 mM iron as Fe_2F_5 in aqueous DMPO and hydrogen peroxide.

with 10% iron as Fe_2F_5 or Fe(II) acetate (Figure 6b and c, respectively) caused cytotoxic responses comparable to that of untreated carbon, at 40−100% and 25−100% cell death (12-h exposure), respectively. However, when the Flammruss was impregnated with a mixture of Fe(II) acetate and Fe(III) nitrate, a smaller proportion of cells ~25−50% died. The trends at other exposure times are similar.

Results of the LDH cytotoxicity assays on Fe_2F_5 and iron salts (without the carbon) added to the media containing the cells are shown in Figure 7. In all cases, the cells were exposed to 3.8, 7.6, and 11.5 μg Fe/mL. Focusing on the 24 h exposure, Fe_2F_5 showed the highest cytotoxic response, at 15−50% cell mortality. Iron(II) acetate caused a cytotoxic response at 15−40%, followed by Fe(III) nitrate at less than 10%. The mixture of Fe(II) acetate and Fe(III) nitrate caused a cytotoxic response at 10−30%.The chelating agent desferoxamine (0.3 mM) reduced the cytotoxic response to Fe_2F_5 by approximately half to a maximum of 20% cell death (Figure 6 in Supporting Information).

Solutions of Fe_2F_5, Fe(II) acetate, and Fe(III) nitrate were made in serum-free cell culture medium at concentrations of 18.5, 42.5, an 14.0 μg of Fe/mL, respectively, and centrifuged to remove any precipitate. None of the solutions showed measurable Fe(II) by the phenanthroline assay. The amount of total iron in solution estimated by atomic absorption spectroscopy ranged from 23.2% of the amount added for Fe_2F_5, followed by Fe(II) acetate at 11.5%, and Fe(III) nitrate at 6.2%.

Discussion

Speciation of Iron on Flammruss and Synthetic Carbon. Though both iron-impregnated Flammruss and iron-loaded synthetic carbon have a mixture of Fe(II) and Fe(III) on their surfaces, as measured by XPS, Flammruss showed little Fenton activity; whereas, synthetic carbon was Fenton active (Figures 2a and 4a). The fact that the iron-loaded Flammruss samples did not show Fenton activity indicates that impregnation leads to tight binding of the iron with the carbon surface, and that Fe(II) is not released into solution. Also, impregnation took place in the Fe(II) form and a significant fraction is oxidized to Fe(III), even though the drying was done under vacuum. In the presence of ascorbate, the iron-loaded Flammruss did become Fenton active. Ascorbate can reduce the Fe(III) and thereby promote Fenton activity (*15*).

The iron-loaded synthetic carbon particles, as synthesized, exhibited Fenton activity, but lost this activity upon standing in water (Figure 4c), with the solution retaining the Fenton activity (Figure 4b). This suggests that the Fenton active species is water-soluble, unlike the Fe(II) on the Flammruss. In an earlier study by Waldman et al. on this synthetic carbon, this solubility aspect of the iron species was not noted (*7, 16*).

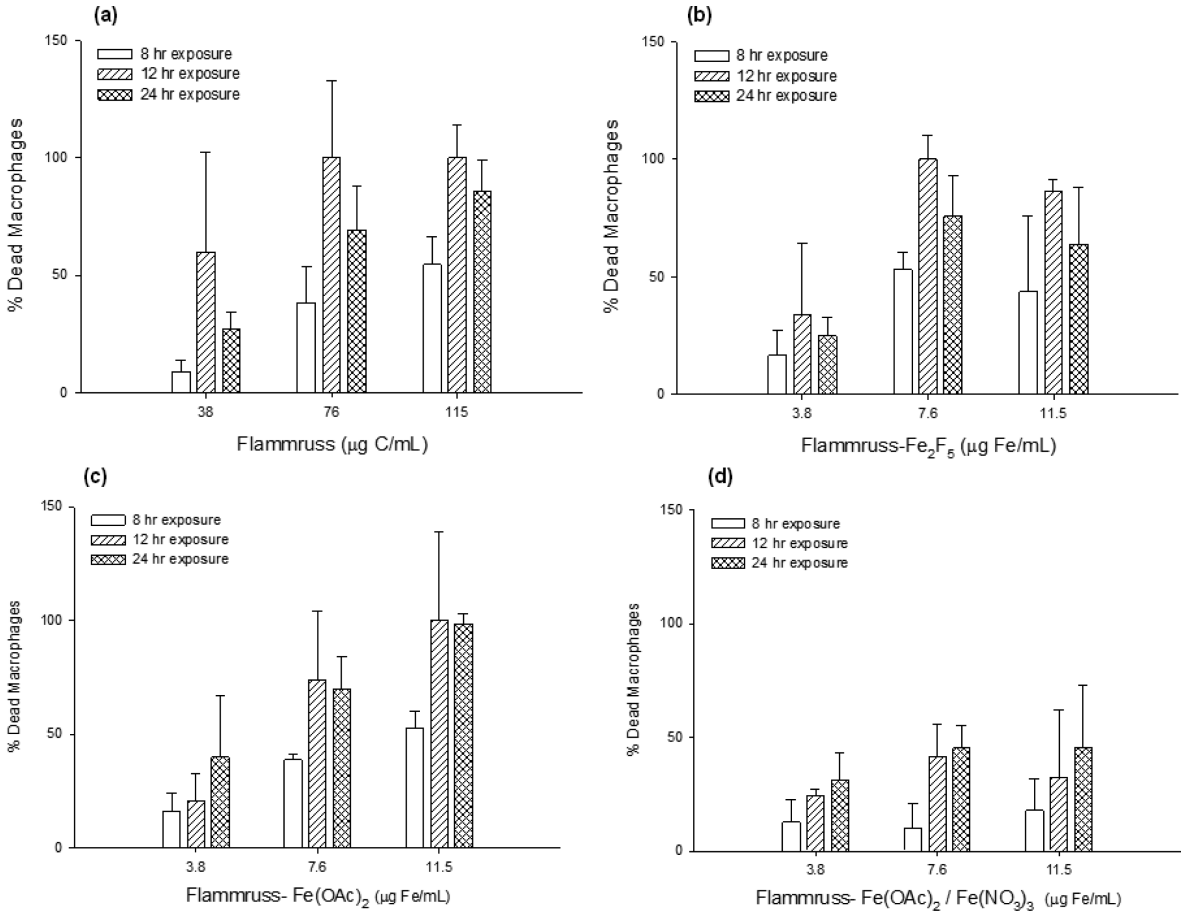

FIGURE 6. Results of cytotoxicity assays for (a) neat Flammruss, (b) Flammruss impregnated with Fe_2F_5, (c) Flammruss impregnated with iron(II) acetate, and (d) Flammruss impregnated with a mixture of iron(II) acetate and iron(III) nitrate. All iron-containing particles were impregnated with 10% iron by weight, total particle loadings were 38−115 μg/mL (well volume 600 μL of media).

Synthesis of iron-loaded synthetic carbon entails pyrolyzing a polymer encapsulated in an iron-exchanged zeolite in argon. On pyrolysis, iron that may have been in the form of Fe(II) or Fe(III) can be reduced to zerovalent iron (*17*). Carbon can also be gasified, reducing iron oxides to zerovalent iron. During etching with hydrofluoric acid, the following reactions can occur (*3, 13, 18*):

$$Fe^0 + 2H_3O^+ \rightarrow Fe^{2+} + 2H_2 + 2^-OH;\ Fe^{2+} \equiv [Fe(H_2O)_6]^{2+} \quad (1)$$

$$4Fe^{2+} + O_2 + 4H^+ \rightarrow 4Fe^{3+} + 2H_2O \quad (2)$$

$$Fe^{2+} + 2F^- \leftrightarrow FeF_2 \quad (3)$$

$$Fe^{3+} + 3F^- \leftrightarrow FeF_3 \quad (4)$$

$$Fe^{3+} + nF^- + (6 - n)H_2O \leftrightarrow [FeF_n(H_2O)_{6-n}]^{(3-n)+} \quad (5)$$

$$[Fe(H_2O)_6]^{2+} + [FeF_5(H_2O)]^{2-} \leftrightarrow Fe_2F_5 \cdot 2H_2O + 5H_2O \quad (6)$$

Low valent iron can be oxidized by reactions such as (1) and (2). The iron species can react with fluoride anion, as in (3) through (5). Mixed-valence species, such as Fe_2F_5 can form as in (6).

Because of the complexity of the above-described iron−fluorine chemistry, and the trace levels of the iron species, we were unable to identify the molecular nature of the species formed on the synthetic carbon surface. However, since Fe_2F_5 is a likely candidate formed during the etching, we synthesized this compound. Upon dissolution of Fe_2F_5, it is known that the cationic species is Fe^{2+} and the anionic species is $[FeF_5(H_2O)]^{2-}$ (*13*). The Fenton activity of Fe_2F_5 observed in Figure 5 stems from the presence of Fe^{2+}. We propose that the Fenton activity observed in the iron loaded synthetic carbon (Figure 4a) also arises from mixed-valence iron fluorides such as Fe_2F_5 that are formed during etching and can be released into the solution, though we have no definite proof that Fe_2F_5 is the active species.

Correlation of Cytotoxicity with Speciation. Iron(II) acetate, Fe(III) nitrate, and Fe_2F_5 added directly to cell culture media containing the macrophages led to different cytotoxic responses (Figure 7), with the trend being Fe_2F_5 > Fe(II) > Fe(III). In all three systems, there was no Fe(II) in solution detectable by the phenanthroline assay. Atomic absorbance spectrometry indicated that the Fe_2F_5 solution contained 23.2% of its original iron content, followed by Fe(II) acetate with 11.5% and Fe(III) nitrate with 6.2%. These studies were done with buffer at pH 7.4, where the existence of free Fe(II) and Fe(III) is unfavorable (*3*). In addition, the presence of phosphate in the buffer can promote autoxidation of Fe(II) and precipitation of iron phosphates (*19*). We propose that the higher level of soluble iron observed in case of Fe_2F_5 is due to the fluoride ligand that helps to stabilize the iron against hydrolysis and colloid formation (*20*). Addition of desferoxamine reduces the toxicity of Fe_2F_5 by half, also indicating that soluble Fe(III) is present in the medium.

There was a strong cytotoxic response to Flammruss at all the loading levels (Figure 6a). Flammruss exhibits a

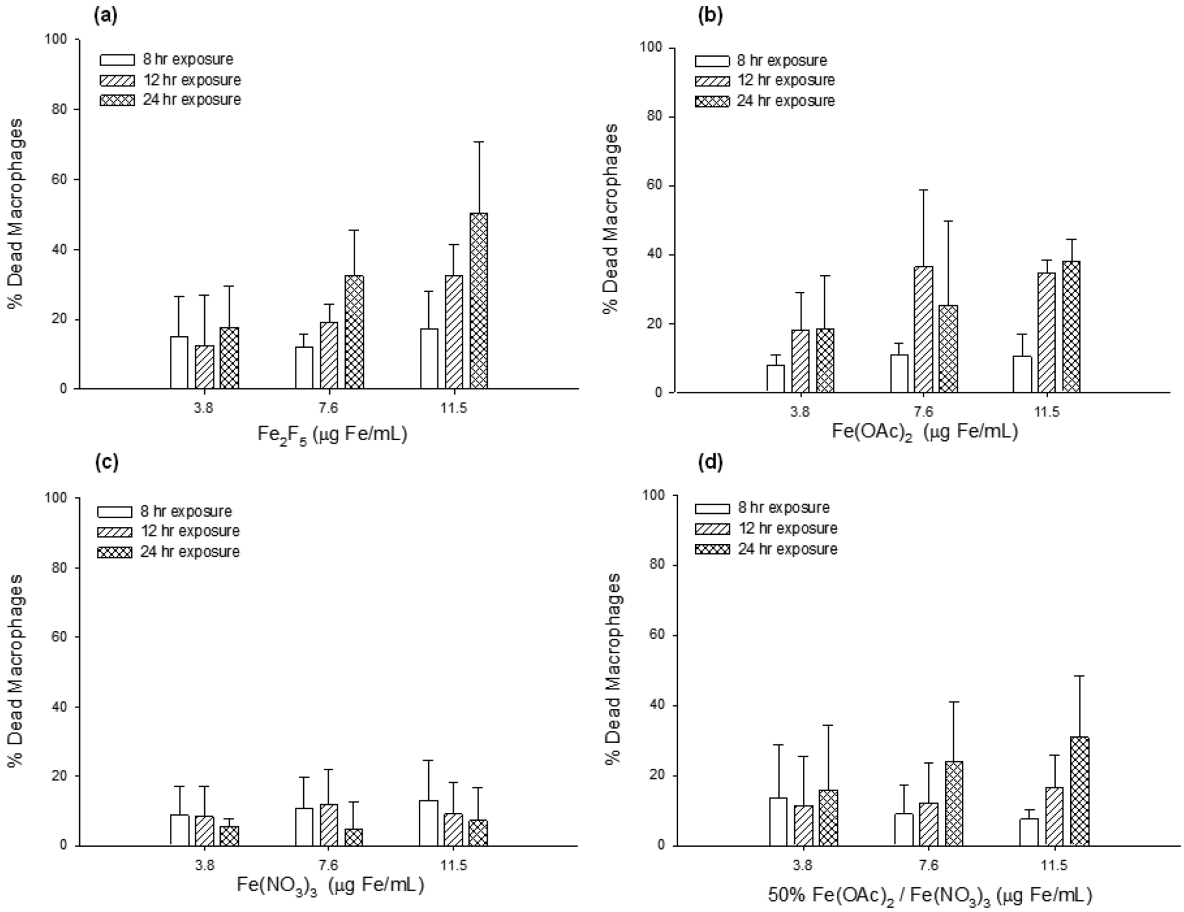

FIGURE 7. Results of LDH cytotoxicity assays for (a) Fe_2F_5, (b) Iron(II) acetate, (c) Iron(III) nitrate, and (d) a mixture of iron(II) acetate and iron(III) nitrate that contains equal part iron(II) and iron(III).

broad peak in EPR at $g = 2.0112$, due to free radicals. One possible route of toxicity is that these radicals react with atmospheric oxygen, forming peroxyl radicals that cause lipid peroxidation and cytotoxicity (*9, 21*). The Fe_2F_5 impregnated Flammruss exhibited comparable cytotoxicity to the parent sample, whereas Fe(II) was slightly decreased, with Fe(III) incorporation resulting in considerably lower cytotoxicity. Light scattering studies show that iron impregnation leads to agglomeration, and the decreased surface area of the iron-loaded particles can lower toxicity, thus the expected increase, e.g., with Fe_2F_5, based on the data with the salts alone, is not being realized.

The results were quite different for iron-loaded synthetic carbon particles. Increased inflammatory responses following exposure of iron-loaded synthetic carbon nanoparticles to human macrophages was noted (*7, 16*). In addition, the Fenton chemistry of the iron-loaded synthetic carbon was significantly higher than that of carbon. Based on the present study, this biological activity of the iron-loaded synthetic carbon possibly arises from soluble fluoroiron species formed during the etching step, a fact we did not recognize in the earlier papers (*7, 16*).

The contribution of compounds such as Fe_2F_5 to environmental toxicity is unclear. Iron fluorides are produced in the steel industry as byproducts of the pickling process (*20*). Fluoride is also present in drinking water, but at low enough concentration that formation of iron fluorides is not expected. Even with that caveat, this study suggests that speciation of iron present on environmentally relevant particles and its bioavailability are the determining factors in their toxicity, and elemental analysis or even the valence state is not a sufficient predictor of toxicity.

Acknowledgments

We acknowledge funding from NIOSH Grant R01 OH009141.

Supporting Information Available

All of the characterization data on Fe_2F_5 and the cytotoxicity in the presence of desferoxamine. This information is available free of charge via the Internet at http://pubs.acs.org/.

Literature Cited

(1) Oberdörster, G.; Stone, V.; Donaldson, K. Toxicology of nanoparticles: A historical perspective. *Nanotoxicology* **2007**, *1* (1), 2–25.
(2) Ghio, A. J. Disruption of iron homeostasis and lung disease. *Biochim. Biophys. Acta* **2009**, *1790*, 731–739.
(3) Pignatello, J. J.; Oliveros, E.; MacKay, A. Advanced oxidation processes for organic contaminant destruction based on the Fenton reaction and related chemistry. *Crit. Rev. Environ. Sci. Technol.* **2006**, *36*, 1–84.
(4) Roper, J. M.; O'Reilly, M. A. Cell-type restrictive responses to chronic oxidative stress. *Curr. Respir. Med. Rev.* **2006**, *2*, 313–319.
(5) Guo, L.; Morris, D. G.; Liu, X.; Vaslet, C.; Hurt, R. H.; Kane, A. B. Iron bioavailability and redox activity in diverse carbon nanotube samples. *Chem. Mater.* **2007**, *19*, 3472–3478.
(6) Dellinger, B.; Pryor, W. A.; Cueto, R.; Squadrito, G. L.; Hegde, V.; Deutsch, W. A. Role of free radicals in the toxicity of airborne fine particulate matter. *Chem. Res. Toxicol.* **2001**, *14* (10), 1371–1377.
(7) Kristovich, R.; Knight, D. A.; Long, J. F.; Williams, M. V.; Dutta, P. K.; Waldman, W. J. Macrophage-mediated endothelial inflammatory responses to airborne particulates: impact of particulate physicochemical properties. *Chem. Res. Toxicol.* **2004**, *17*, 1303–1312.

(8) Hall, W.; Kim, S.; Zubieta, J.; Walton, E. G.; Brown, D. B. Structure of a mixed valence iron fluoride, $Fe_2F_5 \cdot 2H_2O$. *Inorg. Chem.* **1977**, *16* (8), 1884–1887.
(9) Peña, J. M.; Allen, N. S.; Edge, M.; Liauw, C. M.; Hoon, S. R.; Valange, B.; Cherry, R. I. Analysis of radical content on carbon black pigments by electron spin resonance: influence of functionality, thermal treatment, and adsorption of acidic and basic probes. *Polym. Degrad. Stab.* **2001**, *71*, 153–170.
(10) Graat, P. C. J.; Somers, M. A. J. Simultaneous determination of composition and thickness of thin iron-oxide films from XPS Fe 2p spectra. *Appl. Surf. Sci.* **1996**, *100/101*, 36–40.
(11) Long, J. F.; Waldman, W. J.; Kristovich, R.; Williams, M.; Knight, D.; Dutta, P. K. Comparison of ultrastructural cytotoxic effects of carbon and carbon/iron particulates on human monocyte-derived macrophages. *Environ. Health Perspect.* **2005**, *113* (2), 170–174.
(12) Brown, D. B.; Walton, E. G.; Dilts, J. A. Thermal reactions of the mixed-valence iron fluorides, $Fe_2F_5 \cdot nH_2O$. *J. Chem. Soc., Dalton Trans. (1972-1999)* **1980**, *6*, 845–850.
(13) Walton, E. G.; Corvan, P. J.; Brown, D. B.; Day, P. Spectroscopic and magnetic studies of a mixed-valence iron fluoride, $Fe_2F_5 \cdot 7H_2O$. *Inorg. Chem.* **1976**, *15* (7), 1737–1739.
(14) Milićev, S.; Rahten, A.; Borrmann, H.; Šiftar, J. Proton tunnelling in hydrazinium cations: vibrational spectra of $(N_2H_5)_2$-$HGaF_6 \cdot 2H_2O$ and $(N_2H_5)_2HFeF_6 \cdot 2H_2O$ and crystal structure of $(N_2H_5)_2HFeF_6$ at various temperatures. *J. Raman Spectrosc.* **1997**, *28*, 315–321.
(15) Roden, E. E. Analysis of long-term bacterial vs. chemical Fe(III) oxide reduction kinetics. *Geochim. Cosmochim. Acta* **2004**, *68* (15), 3205–3216.
(16) Waldman, W. J.; Kristovich, R.; Knight, D. A.; Dutta, P. K. Inflammatory properties of iron-containing carbon nanoparticles. *Chem. Res. Toxicol.* **2007**, *20*, 1149–1154.
(17) Yang, J.; Mori, T.; Kuwabara, M. Mechanism of carbothermic reduction of hematite in hematite-carbon composite pellets. *ISIJ Int.* **2007**, *47* (10), 1394–1400.
(18) Fernando, L. A. Solution chemistry of HNO_3/HF pickle mixtures. *Metall. Trans. B* **1990**, *21B*, 5–9.
(19) Welch, K. D.; Davis, T. Z.; Aust, S. D. Iron autoxidation and free radical generation: effect of buffers, ligands, and chelators. *Arch. Biochem. Biophys.* **2002**, *397* (2), 360–369.
(20) Gálvez, J. L.; Dufour, J.; Negro, C.; López-Mateos, F. Fluoride speciation in stainless steel pickling liquor. *ISIJ Int.* **2006**, *46* (2), 281–286.
(21) Wright, J. S.; Shadnia, H.; Chepelev, L. L. Stability of carbon-centered radicals: effect of functional groups and energetics of addition of molecular oxygen. *J. Comput. Chem.* **2009**, *30* (7), 1016–1026.

ES101250S